

Article

High-Performance Multiple-Input Multiple-Output Antenna System For 5G Mobile Terminals

Mujeeb Abdullah ¹, Saad Hassan Kiani ², Lway Faisal Abdulrazak ³, Amjad Iqbal ^{4,*},
M. A. Bashir ⁵, Shafiullah Khan ⁶ and Sunghwan Kim ^{7,*}

¹ Department of Computer Science, Bacha Khan University, Charsadda 24420, Pakistan; mujeeb.abdullah@gmail.com

² Electrical Engineering Department, Iqra National University, Peshawar 25000, Pakistan; iam.kiani91@gmail.com

³ Computer Science Department, Cihan University Slemani, Sulaimaniya 46002, Iraq; lway.faisal@sulicihan.edu.krd

⁴ Centre For Wireless Technology, Faculty of Engineering, Multimedia University, Cyberjaya 63100, Malaysia

⁵ School of Electronic Science and Engineering, University of Electronic Science Technology China, Chengdu 611731, China; adil.bashir@yahoo.com

⁶ Department of Electronics, Islamia College University, Peshawar 25000, Pakistan; shafielectron@yahoo.com

⁷ School of Electrical Engineering, University of Ulsan, Ulsan 44610, Korea

* Correspondence: aiqbal@ieee.org (A.I.); sungkim@ulsan.ac.kr (S.K.); Tel.: +82-52-259-1401 (S.K.)

Received: 25 August 2019; Accepted: 22 September 2019; Published: 25 September 2019



Abstract: In this paper, the systematic design of a multiple antenna system for 5G smartphone operating at 3.5 GHz for multiple-input multiple-output (MIMO) operation in smartphones is proposed. The smartphone is preferred to be lightweight, thin, and attractive, and as a result metal casings have become popular. Using conventional antennas, such as a patch antenna, Inverted-F antennas, or monopole, in proximity to metal casing leads to decreasing its total efficiency and bandwidth. Therefore, a slot antenna embedded in the metal casing can be helpful, with good performance regarding bandwidth and total efficiency. The proposed multiple antenna system adopted the unit open-end slot antenna fed by Inverted-L microstrip with tuning stub. The measured S-parameters results agree fairly with the numerical results. It attains 200 MHz bandwidth at 3.5 GHz with ports isolation of (≤ -13 dB) for any two antennas of the system. The influence of the customer's hand for the proposed multiple antenna system is also considered, and the MIMO channel capacity is computed. The maximum achievable MIMO channel capacity based on the measured result is 31.25 bps/Hz and is about 2.7 times of 2×2 MIMO operation.

Keywords: 5G antenna; slot antenna; mobile terminal antenna; MIMO antenna

1. Introduction

With evolving semiconductor technology, the electronic communication components can be easily packed closely to design compact structures with high processing capabilities, such as a smartphones and wireless routers [1]. Hence, multiple antenna structures use high processing capability efficiently and boost data throughput. As such, 2×2 multiple-input multiple-output (MIMO) devices are extensively studied and commercialized for modern cellular technology. Moreover, most of the focus of the research was dedicated to the reliability of the link. However, the availability and advancement of computing combined with the upgraded radio propagation system or antenna system will open up the mobile internet of things (IoT) and enhance the data rate. Most recently, Ericsson, Telstra, and Qualcomm Technologies have demonstrated 4×4 MIMO operation, an opening step towards download speeds of 1 Gbps in the commercial network [2]. This processing capacity can

be further enhanced to 8×8 MIMO and 16×16 MIMO configuration for a future 5G smartphone. Such configurations will require multiple antenna systems accommodating more than four antenna elements. As a result, most of the reported work in [3–6] on multiple antenna structure work is limited to the frequency band for 2G/3G/4G. In [3], the two antenna elements are oriented diagonally at the printed circuit board of volume of $110 \times 65 \times 0.8 \text{ mm}^3$, and each antenna has dimensions of $24 \times 14.5 \text{ mm}^2$. The two antennas are decoupled by employing ground slots and inverted-L ground branches etched at the bottom layer of the substrate. As the antenna decoupling mechanism required a large space and extended microstrip feeding mechanism, this resulted in limited prospects to be employed for massive MIMO.

In [4], the four-antenna structure is implemented with the main antenna operating for LTE 700/2300/2700 MHz UMTS/GSM 800 MHz /WLAN bands with dimensions of $65 \times 9.5 \text{ mm}^2$ and three auxiliary antennas operating at 1800 to 2700 MHz with a dimension of $40 \times 6 \text{ mm}^2$. Also in [5], a multiple antenna system is realized by employing four printed monopoles at the four corners of the printed circuit board for the UMTS frequency band. The printed circuit board dimensions are $95 \times 60 \times 0.8 \text{ mm}^3$. The occupied area for each antenna element is comparable to the operating wavelength, and the minimum isolation between antenna elements is less than 11 dB. As a result, the above-reported structure [3–5] has an inherent limitation of its size and a complicated antenna isolation structure. An attempt is made to realize a multiple antenna system as discussed in [6–8]. In [6], a multiple antenna system is realized on a circuit board of size $115 \times 65 \times 0.8 \text{ mm}^3$, with each unit antenna having dimensions of $16 \times 7.42 \text{ mm}^2$ and a minimum isolation of greater than 10 dB with the operating frequency band of 2 GHz. In [7], the multiple antenna system is investigated by using an unit antenna element with dimensions of dielectric cube $10 \times 10 \times 5 \text{ mm}^3$ with the printed circuit board of FR-4 substrate of the dimensions $136 \times 68.8 \times 1 \text{ mm}^3$. The antenna element is a three-dimensional inverted-F antenna wrapped around the said cube. The unit antenna operates at frequency bands for GSM1900, LTE2300, 2.4-GHz WLAN, and LTE2500. Small antenna cubic elements were proposed for MIMO operation at LTE bands [9]. As the maximum isolation between the middle and the top antenna element is 10 dB, this results in limited practical application. In summary, the antenna system discussed mainly focused on the GSM/UMTS frequency band of operation in low radio frequency bands [3–8,10–14]. Moreover, accommodating multiple antennas at the low-frequency band is a daunting task on a limited footprint area of a smartphone due to the transfer of power among ports.

To counter this difficult task, the World radio conference 2015 (WRC-2015) allocated new frequency bands for 5G cellular technology consisting of sub-6 GHz or below 6 GHz (2.6/3.5 GHz bands [15]). Slot antennas have been proposed for multiband operation below 3GHz [16–19]. Therefore, it motivates this work to propose new multiple antenna systems for smartphone operating in the radio spectrum Sub-6 GHz band (3.5 GHz). The proposed multiple antenna system is based on a unit slot antenna structure with ease of integration in the modern trend of smartphone and adequate performance measure compared to the inverted-F antenna [20]. The MIMO performance measures, such as envelope correlation coefficient (ECC), mean effective gain (MEG), and MIMO channel capacity, and customer's hand effect are studied extensively for the proposed multiple antenna system.

2. Antenna Geometry

The detailed design procedure of the six open-end slot antenna system is discussed in this section. The main circuit board or Printed circuit board (PCB) supporting the proposed multiple antenna system consists of FR-4 substrate with relative permittivity of 4.4 and loss tangent of 0.02. The dimensions of PCB are $136 \times 68 \times 1.6 \text{ mm}^3$, as shown in Figure 1. To swiftly accommodate (2G/3G/4G) antennas, space reservation is made. The dimensions of each open-end slot antenna are $8.5 \times 3 \text{ mm}^2$ fed by microstrip with tuning stub, also referred to as inverted-L microstrip feed. The tuning stub is helpful to effectively couple electromagnetic energy to the antenna.

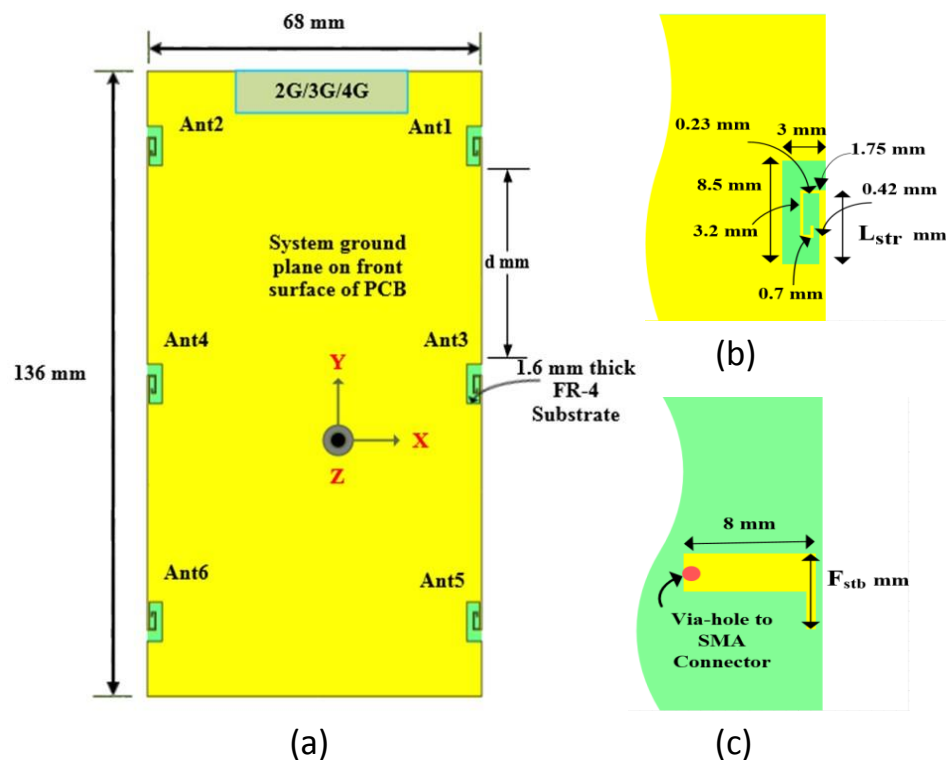


Figure 1. (a) The multiple antenna system for multiple-input multiple-output (MIMO) application in a smartphone. (b) Geometric configuration of unit slot antenna. (c) Inverted-L feeding strip.

3. Results and Discussions

The detailed analysis of the proposed multiple antenna system or multiple antenna system is carried out with commercial electromagnetic software, namely Computer Simulation Technology (CST) Microwave Studio. The design of the proposed multiple antenna system evolved from an open-end rectangular shape slot etched at the top edge, called the reference antenna or Ref_Ant, and fed by the inverted-L microstrip printed on the opposite side of the substrate. The fabricated MIMO antenna system is shown in Figure 2 with corresponding simulated scattering parameters are depicted in Figure 3. As evident with the length of 8 mm, the unit slot or the Ref_Ant1 failed to operate for the desired band of 3.5 GHz for Figure 3a. The slot antenna is usually treated as a magnetic dipole, with its first resonating frequency depending on its electric length. The resonating behavior of the unit slot antenna can further be studied by considering the input impedance depicted in Figure 3b. The dominating inductive impedance is effectively subdued by adding a parasitic strip with more capacitive behavior and referred to as Prop_Ant.

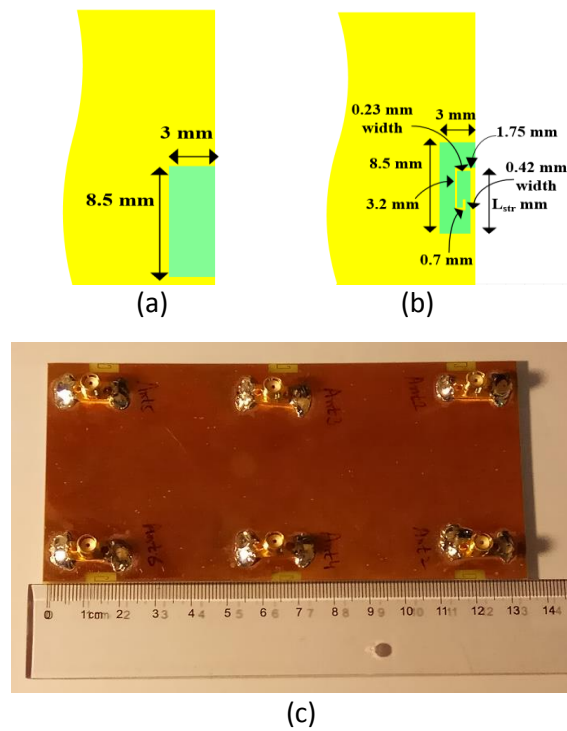


Figure 2. (a) The unit slot antenna Reference Antenna or Ref. Ant. (b) Proposed Antenna or Prop_Ant (Ant1). (c) Fabricated multiple antenna system.

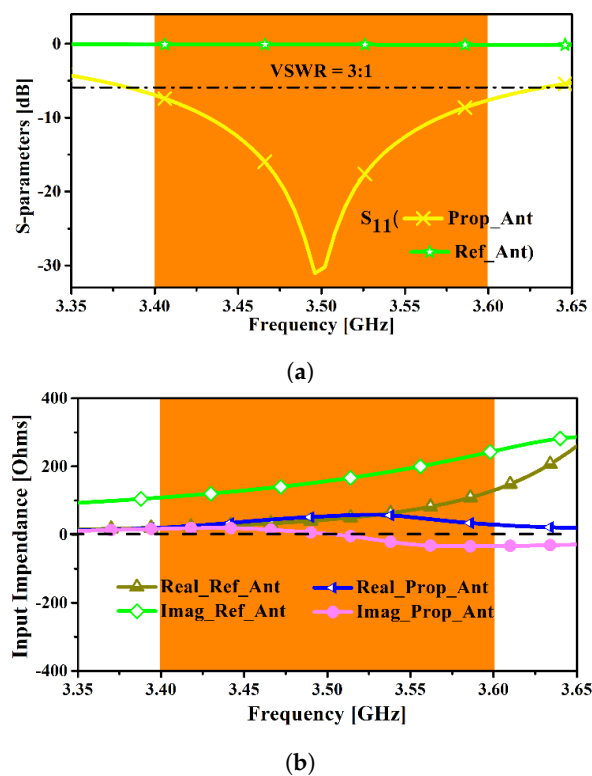


Figure 3. (a) Simulated Scattering S-Parameters for the unit slot antenna. (b) Input impedance curve.

Initially, for a unit slot or Ref_Ant, pivotal geometric parameters such as L_{str} mm (parasitic strip length) and F_{stb} (Feeding strip length) are studied extensively. The design process of the multiple antenna system is further studied extensively by considering parameters F_{stb} , L_{str} , and d mm. The parameter F_{stb} of the feeding strip plays an important role together with the parasitic strip.

Varying the feeding strip length of $F_{stb} = 4.5$ mm to 5.5 mm improves the electromagnetic coupling, or more specifically Prop_Ant, which will resonate at 3.5 GHz, as shown in Figure 4a. Also, when the value of L_{str} is varied from 5 mm to 5.8 mm the resonating frequency of the unit slot, open-end antenna, decreases as depicted in Figure 4b. The mutual interaction between antenna elements in the system is quantified by studying the parameter d mm for Ant1, Ant3, and Ant5. The scattering parameters of interest, S_{31} and S_{51} , are given in Figure 4c. The other S-parameters are well below -25 dB. Hence, they are not plotted for clarity. With a minimum value of $d = 15.25$ mm, the S_{31} is more than -9.8 dB. Increasing the distance between two antennas, with $d = 43.5$ mm or the middle position of the ground plane, can help to increase the dominating S_{31} to -13 dB, as illustrated in Figure 4c. Furthermore, an inter-spacing between antenna elements greater than $\lambda_g/2$ (λ_g is guided wavelength at 3.5 GHz) results in better isolation, which is enough to ensure independent behavior of each antenna with less mutual coupling.

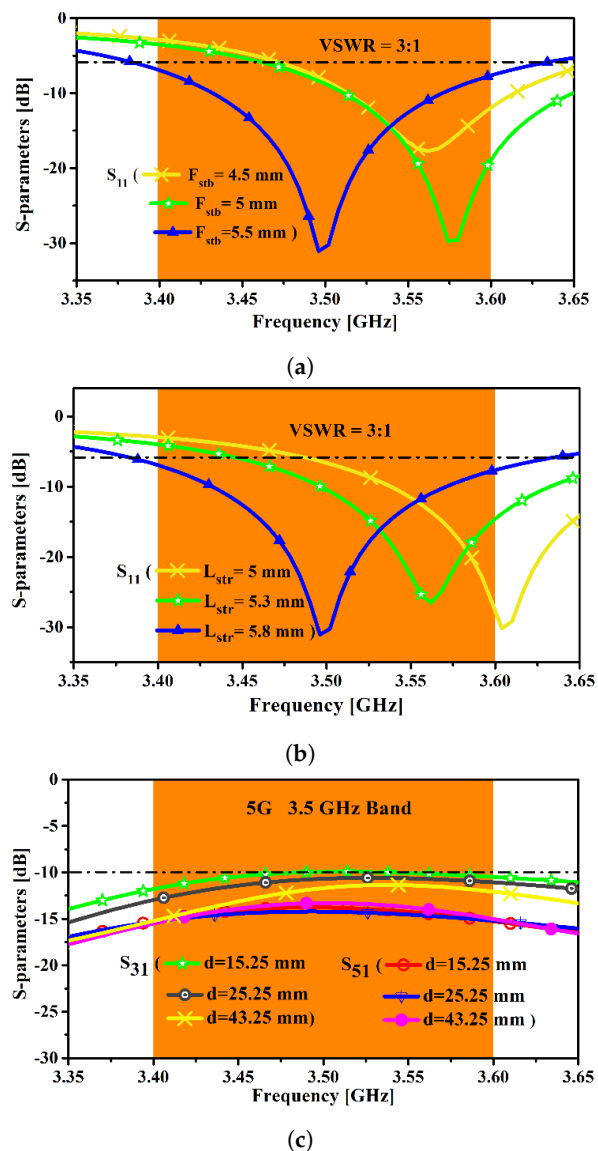


Figure 4. The simulated S-parameter as a function of (a) F_{stb} , (b) L_{str} , and (c) d .

4. Measured Results

4.1. S-Parameters

The proposed multiple antenna system for MIMO operation is fabricated as depicted in Figure 2c. The measurement of scattering parameters is acquired with Agilent Network analyzer N5247A, in such a manner that the two antennas under study are connected to a vector network analyzer while the corresponding antennas are connected to an impedance load of 50 Ω . Due to the symmetric configuration of the structure and for clarity, the scattering parameters or (S-parameters) are only discussed for Ant1, Ant3, Ant5, which are shown in Figure 5. Fair agreement between the simulated and measured results can be observed.

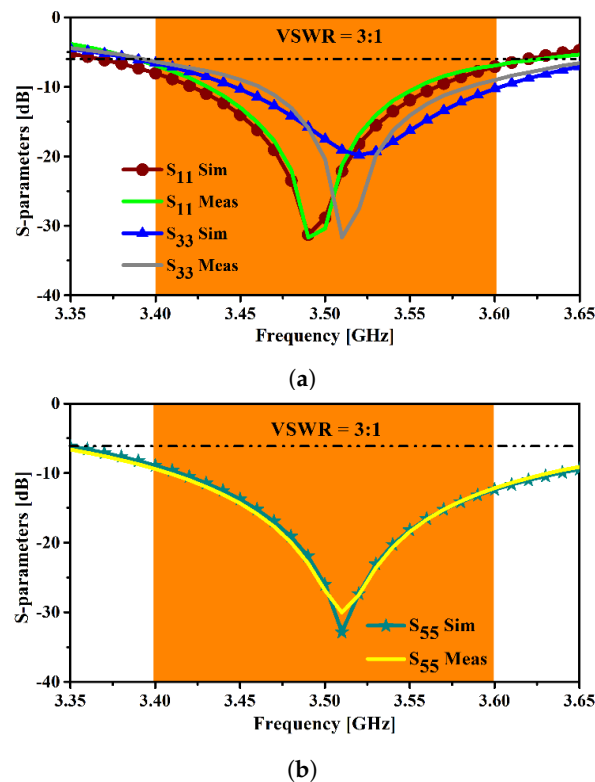
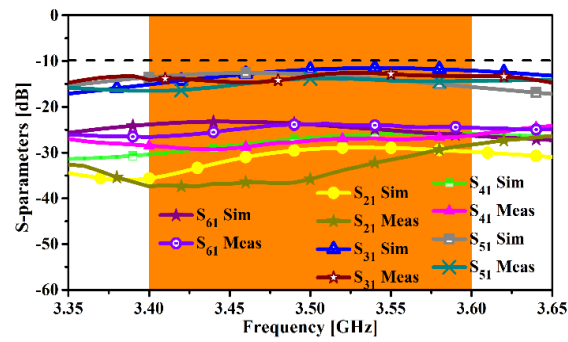


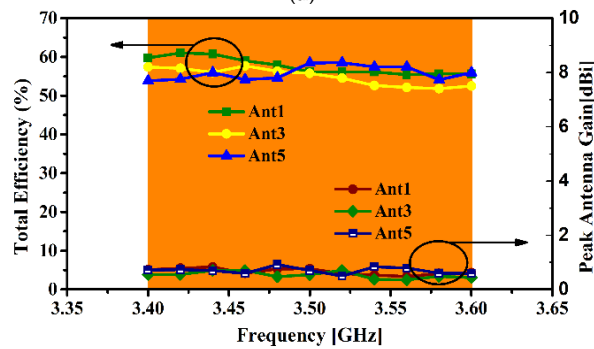
Figure 5. The S-Parameters; Simulated is denoted by (Sim) and Measured by (Meas). (a) Ant1 and Ant3. (b) Ant5.

The slight difference between measured and simulated results for Ant1 and Ant3 may be attributed to the tolerance of the SMA connector, the termination resistance, and the contribution of hand soldering. The measured impedance bandwidth obtained based on V.S.W.R 3:1 is 200 MHz from 3400 MHz to 3600 MHz. The mutual coupling between unit open-end slot antennas with other antennas is better than 12.5 dB, as shown in Figure 6a.

The measured total efficiencies at Ant1, Ant3, and Ant5 are 58% to 50%, 55% to 48%, and 55% to 49%. The corresponding gains at the Ant1, Ant3 are 3.2 and 4.8 dBi respectively, and for Ant5 it is 3 dBi, as shown in Figure 6b.



(a)



(b)

Figure 6. (a) The measured and simulated S-Parameters for port isolation. (b) Measured gain and total efficiency for Ant1, Ant3, and Ant5.

4.2. Radiation Pattern

The far-field measurements such as total efficiencies (including the mismatching losses) of the proposed multiple antenna system are carried out in the anechoic Star lab SATIMO chamber. For each total efficiency measurement, the other corresponding antenna elements were connected to a 50 Ω load. As discussed earlier, due to the symmetric configuration the measured radiation patterns for Ant1, Ant3, and Ant5 are discussed.

The radiation pattern with directive gains is depicted in the x-y plane in Figure 7 for Ant1, Ant3, and Ant5. In the x-y plane for the Ant1 and for Ant5, the radiation pattern is nearly quasi-omnidirectional, with a dip null at $\phi = 210$ and $\phi = 150$ respectively. The Ant3 radiation pattern is nearly omnidirectional. The Ant1, Ant3, and Ant5 are directives in the +x-axis. The slot and antennas are planar and by necessity have a pure linear polarization in the plane of the antenna, in this case, the x-y plane. The measured level of the cross polarization is less than -28 dB in the main radiation direction.

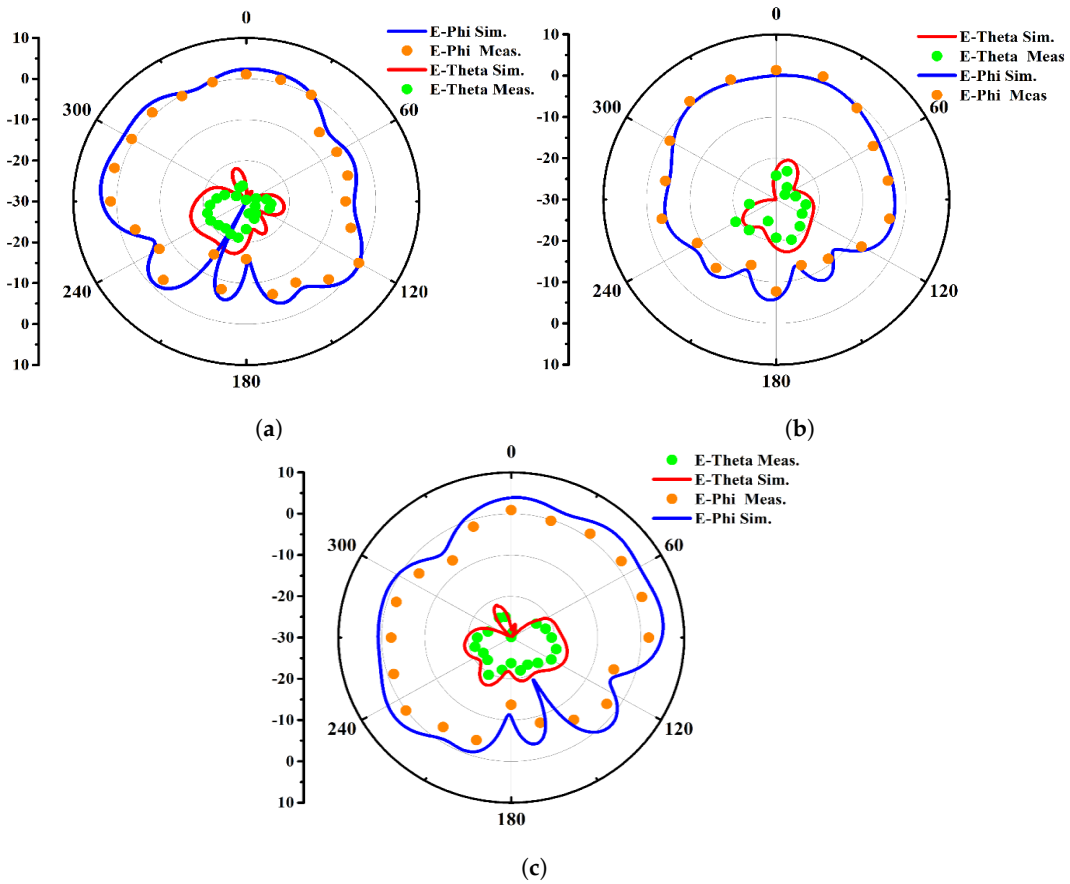


Figure 7. Measured and simulated radiation pattern x-y plane for (a) Ant1, (b) Ant3, and (c) Ant5.

4.3. Surface Current and Electric Field Distribution

The study of surface current distribution is helpful to grasp the radiating behavior of the unit antenna and is discussed in this section. The unit slot antenna is excited by the inverted-L shape microstrip feed printed on the back of PCB. As strong current intensity is observed at the parasitic strip, the close and inner end of the slot is shown in Figure 8a.

Also, depicted in Figure 8b, for Port 1 excitation the electric field anti-nodes will be located in the middle of the slot and the field node position is at the end of the slot. Hence, the antenna evolves into the open-end slot monopole, and the antenna size is reduced.

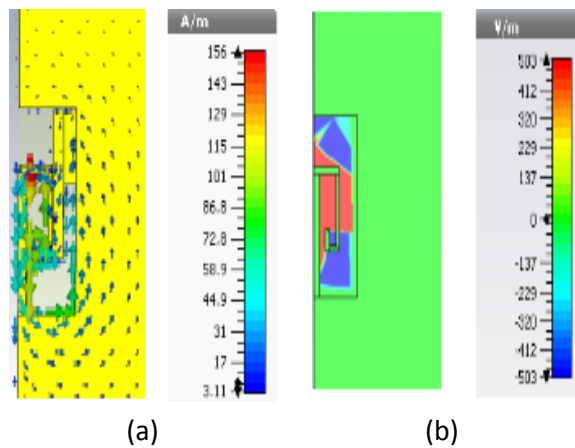


Figure 8. The unit antenna element or Ant1 simulated at 3.5 GHz. (a) Current distribution. (b) Electric field distribution.

4.4. Customer's Hand Effect

In this section, the customer's hand effect on the performance of the multiple antenna system is studied, with a focus on data mode operation. Furthermore, this section will also consider the Envelope Correlation Coefficient (ECC) for the customer hand effect. The study of the customer hand effect is an essential requirement to assess its influence on the performance antenna elements. The main factors affecting the hand are as follows: antenna (design, size, location) and handgrip (position of the fingers concerning antenna, obstructed antenna area, palm-hand distance). The positions or grip style used in this study are by the Cellular Telecommunications Industry Association (CTIA) standards version 3.4 [21].

Accordingly, the electric properties of hand phantom or customer's hand are modeled as reported in [22] across the desired 3.5 GHz Band. The target value is a real part of permittivity 28 to 32 and the effective conductivity is 0.7 to 0.9 S/m for hand phantom, depicted in Figure 9. However, for this study, we model the customer's or user's hand with a constant value interpolated at the center frequency of 3.5 GHz with effective permittivity of 29 and effective conductivity of 0.8 S/m. The two postures considered for this study are Single-Hand Operation (SHO) and Two-Hand Operation (THO), depicted in Figure 9. Two- or dual-hand operation is not yet standardized, hence the posture adopted in this study is inspired by that which is mostly used by customers.

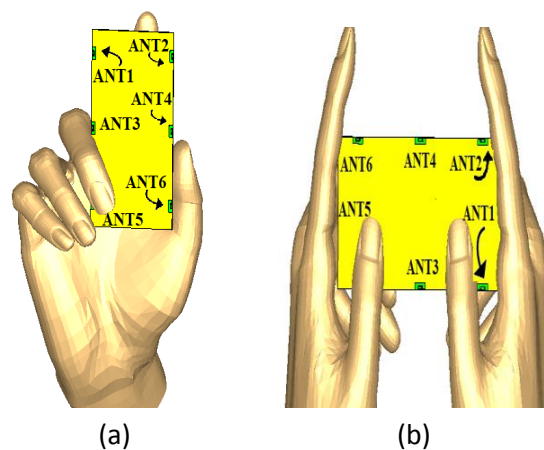


Figure 9. The customer's hand usage scenarios: (a) Single-Hand Operation (SHO) and (b) Two-hand Operation (THO).

The total efficiency of the proposed multiple antenna system in free space is illustrated in Figure 10 and a comparison of the total efficiency of the single antenna element with reference to a multiple antenna system is presented. The single antenna element total efficiency varies from 60% to 70%. On the other hand, for the antenna elements in the other system the average total efficiency varies on average from 45% to 57%. The corresponding total efficiencies and ECC for the SHO and THO are presented in Figures 11 and 12 respectively. As for the SHO mode, the customer's palm being near a smartphone resulted in a decrease in total efficiency from Ant3 to Ant6 to below 50%. The customer's hand will lead to dielectric loading of the antenna system. Thus, it reduces the total efficiency depending on the proximity of the hand to the antenna, with the details reported in [23]. Recently, different techniques have been proposed to mitigate the user hand effect. In [24,25], a thick buffer material with high permittivity or dielectric constant with low loss or low conductivity was used to counter the near-field coupling of the radiating antenna with the hand. This technique needs extra volume.

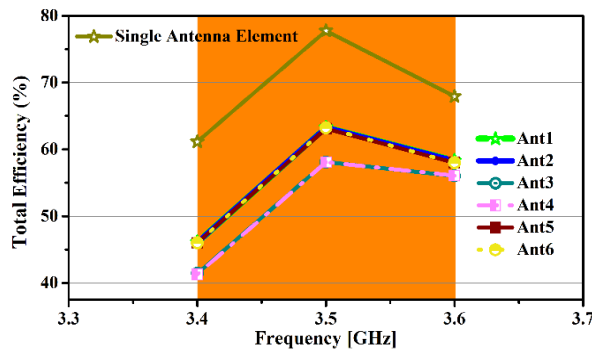
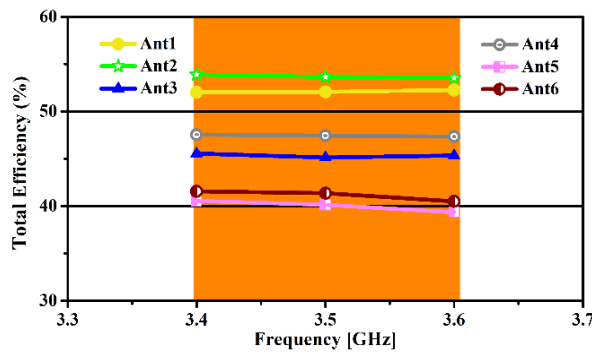
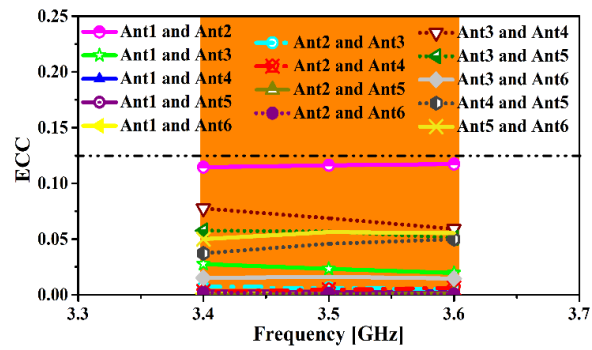


Figure 10. The total efficiency of the multiple antenna system free spaces (without the customer’s hand).



(a)



(b)

Figure 11. Single-Hand Operation (SHO) for the proposed multiple antenna system. (a) total efficiency. (b) Envelope correlation coefficient.

Furthermore, in [26] the authors dynamically selected the antenna with the best performance metrics in the presence of the user’s hand for a mobile terminal. The simulated Envelope correlation coefficient for the desired scenarios of SHO and THO is depicted in Figure 12b, and is lower than 0.5 as required for MIMO operation. Aside from the above-mentioned techniques, the user hand effect mitigated by using passive circuit components or tuning circuit is classified as adaptive impedance matching (AIM) [27].

AIM with variable impedance is a separate circuit module attached to the antenna to detect the time-varying mismatch. This work studied the direct interaction of the antenna system with the user’s hand and the method discussed in [23,24,26] was applied to reduce the effect of user’s hand dielectric loading of the proposed antenna system.

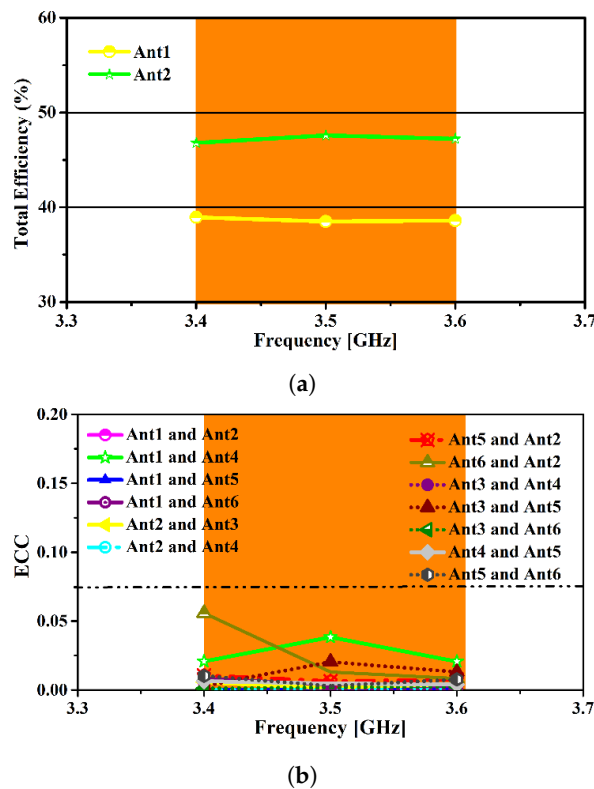


Figure 12. Two-Hand Operation (THO) for the proposed multiple antenna system. (a) total efficiency. (b) Envelope correlation coefficient.

4.5. Key Performance Metrics Evaluation for MIMO Systems

The performance of a smartphone is significantly affected by different hand postures in rich scattering propagation. The critical performance metrics required in such propagation scenarios are Envelope correlation coefficient (ECC) and Mean effective gain (MEG). The propagation environment effects are expressed as a statistical distribution function as explained in [28]. As for optimal MIMO operation, the ECC should be less than 0.5 to quantify the independent behavior of each antenna in the multiple antenna system. It is calculated from either S-parameters [29] or 3-D radiation pattern [30,31] for the far-field zone of multiple antenna structure. In this work, the ECC, MEG, and MIMO channel capacities are calculated based on the measured result conducted from the far-field measurements in the starlab anechoic chamber. ECC and MEG are calculated from the measured results according to [28]. Most studies reported in [32] considered $\Gamma = 0$ dB for indoor and $\Gamma = 5$ dB for outer door fading environment. The ECC as given in (1) and MEG in (2) are calculated from the measured results according to [32], given as:

$$ECC = \frac{|\iint_{4\pi} (\vec{F}_i(\theta, \phi)) \times (\vec{F}_j(\theta, \phi)) d\Omega|^2}{\iint_{4\pi} |(\vec{F}_i(\theta, \phi))|^2 d\Omega \iint_{4\pi} |(\vec{F}_j(\theta, \phi))|^2 d\Omega} \tag{1}$$

where $\vec{F}_i(\theta, \Phi)$ describe the 3D radiation pattern when antenna i is excited and $\vec{F}_j(\theta, \Phi)$ describe the 3D radiation pattern when antenna j is excited. Solid angle in above Equation (1) is represented as Ω .

$$MEG = \int_{-\pi}^{\pi} \int_0^{\pi} \left[\frac{r}{r+1} G_{\theta}(\theta, \phi) P_{\theta}(\theta, \phi) + \frac{1}{1+r} G_{\phi}(\theta, \phi) P_{\phi}(\theta, \phi) \right] \sin\theta d\theta d\phi \tag{2}$$

where $G_{\phi}(\theta, \phi)$ and $P_{\theta}(\theta, \phi)$ are angle of arrival and r is the cross polar ratio which can be expressed as Equation (3).

$$r = 10 \log_{10} \left(\frac{P_{vpa}}{P_{hpa}} \right) \tag{3}$$

where the power received by vertically polarized antenna and horizontally polarized antenna are represented as P_{vpa} and P_{hpa} , respectively.

The ECC calculated based on the measured far-field measurement for the proposed multiple antenna system is well below 0.27, as depicted in Figure 13. The MEG calculation accounts for total efficiency, gain, and the wireless propagation environment to measure the antenna–channel mismatch. For good power balance, the quantity of (MEGi/MEGj) or the difference between MEGs should be less than 3 dB for diversity performance. Terms i and j represent antennas. The MEG calculated based on the measured result is well below 3 dB, as shown in Table 1.

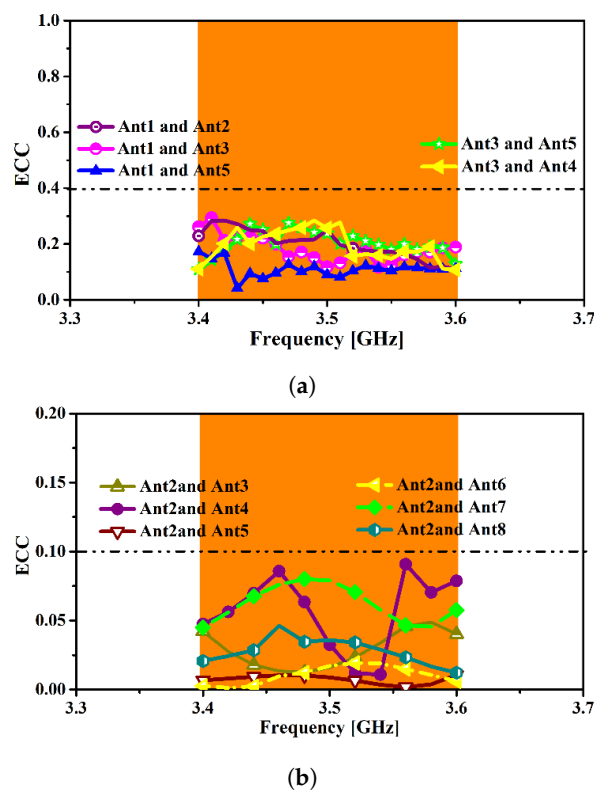


Figure 13. The Envelope Correlation Coefficient (ECC) based on measured far-field results (a) ECC for Ant1 with Ant2, Ant3, Ant4 and Ant5, and (b) ECC for Ant2 with Ant3, Ant4, Ant5, Ant6, Ant7 and Ant8.

The channel capacity is an important parameter to estimate MIMO system performance. The channel capacities for the proposed multiple antenna system to support 6×6 MIMO based on measured total efficiency and ECC is 31.25 bps/Hz. The MIMO channel capacity was calculated based on [32–34]. The MIMO channel capacity was calculated by averaging the 10,000 Rayleigh fading realization with a reference signal to noise ratio (SNR) of 20 dB. The customer hand effect on the operation of the proposed multiple antenna system with respect to ECC and MIMO channel capacity was tabulated in Table 2, based on the simulated data using CST Microwave Studio.

Table 1. Mean Effective Gain (MEG) for Ant1 to Ant6.

Frequency (GHz)	MEG Ant1 (dB)	MEG Ant2 (dB)	MEG Ant3 (dB)	MEG Ant4 (dB)	MEG Ant5 (dB)	MEG Ant6 (dB)
Indoor XPR = 1	−3.20	−3.15	3.20	−3.18	−3.22	−3.13
Indoor XPR = 5	−3.40	−3.50	−3.64	−3.48	−3.50	−3.70

Table 2. MIMO channel capacities and ECC for free space (without hand) and customer’s hand scenarios based on simulated results.

MIMO Configuration	Scenario	ECC	Channel Capacity (bps/Hz)
6 × 6	Free Space	0.012	34.25
	Single-Hand Mode	0.10	27.43
	Two-Hand Mode	0.07	23.24

4.6. Impact of Display Module (Metal Casing and Liquid Crystal Display)

The impact of the display module consists of a metal frame and the Liquid Crystal Display (LCD) is studied in this subsection. The metal frame adheres to the ground and the LCD display is made of glass with reflective permittivity of 7 and loss tangent of 0.02 with overall dimensions 136 mm × 68 mm × 1 mm, as shown in Figure 14. The metal frame section in the display module is extended to the slot radiator due to the fact that it is connected to the ground plane of Printed Circuit board (PCB) can be considered a ground for real phone. As evident from Figure 15, the display module will affect the resonating frequency of the unit antenna or Ant1 and it still meets the required standard of VSWR of 3:1. The ports isolation for the proposed multiple antenna system is greater the 13.5 dB. The tuning parameter of F_{stb} can be used for adjusting the resonating frequency, as given in Figure 16, for a unit slot antenna. Similarly, the other antenna elements can also be tuned to the center frequency of 3.5 GHz.

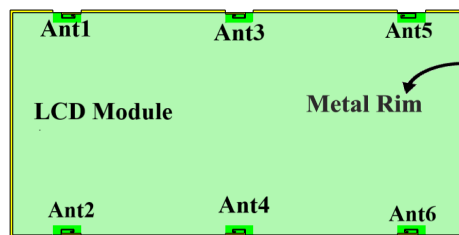
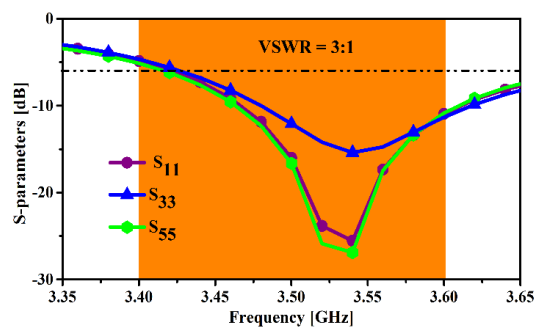
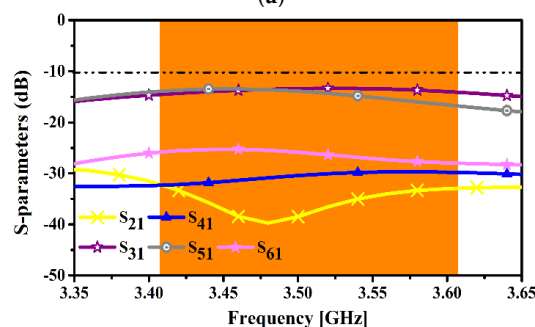


Figure 14. Simulation model for the proposed multiple antenna system with the display module.



(a)



(b)

Figure 15. Simulated S-Parameters (a) Impedance Bandwidth, (b) Ports Isolation.

Table 3 shows the performance comparison between the proposed works and the previous report. As discussed earlier that the most of reported focused on Long term Evolution (LTE) and Global System of Mobile communication frequency band of 700 MHz to 1800 MHz and also in 2 GHz bands. Furthermore, the reported structure is large in dimensions has limited applications to be integrated for 5G Mobile terminal. Hence, the proposed multiple antenna system using the ground plane structure of mobile or slot antenna is easily designed and implemented on the longer edges or sided edges. With the modern trend, od smartphone requires a metal frame structure. Thus the proposed multiple antenna system can be easily embedded in it. As for 2G/ LTE, smooth operation space reservation is made at the top and lower short edges of PCB of the smartphone.

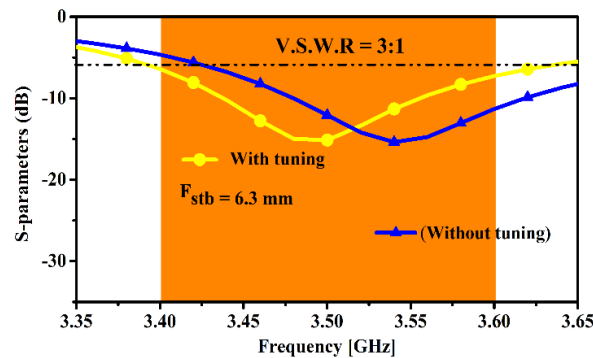


Figure 16. Comparison of simulated S_{11} of Ant1 by tuning the F_{stb} parameter.

Table 3. Performance comparison with smartphone antenna. Abbreviation: Number of Antenna elements = # Ant, Total Efficiency = T.E%, Peak Channel Capacity (bps/Hz) = PCC, Envelope correlation Coefficient = ECC.

Ref.	Bandwidth (GHz)	#Ant	T.E% (meas)	PCC	ECC (required <0.5)
Proposed	3.4–3.6	6	50 to 60	32	0.15
[3]	1.67–2.76	2	70 to 80	Not Given	0.05
[4]	1.7–2.2	4	83 to 89	Not Given	0.02
[5]	0.6–0.9/1.6–2.6	4	40 to 70	Not Given	0.25
[7]	1.8–1.9/2.3–2.6	6	37 to 79	Not Given	0.16
[8]	0.73–0.79/2.3–2.4	4	~70	Not Given	0.4
[13]	0.6–0.9	4	40 to 50	17	0.3

5. Conclusions

This work presented a multiple-input multiple-output, six element, open-ended slot antenna system fed by Inverted-L shaped microstrip with tuning stub for 5G mobile terminals operating at a single band of 3.5 GHz. Three identical antenna elements (open-ended slot) were etched across each length of the chassis and investigated. The impedance bandwidth of 200 MHz achieved, base on -6 dB criteria, enough for a future 5G cellular wireless communication system, with good isolation of <-13 dB using a spacing of half a wavelength among any two radiating elements and having an ECC less than 0.15 and a peak gain of 4.8 dBi. Meanwhile, the effects of the user’s hand in both single-hand and two-hand scenarios was studied and showed good results, with ECCs of 0.10 and 0.007 and channel capacities of 27.43 and 23.24 bps/Hz, respectively. The measured results agreed fairly well with the simulated results. The free space ergodic MIMO channel capacity calculated for the proposed antenna system using Matlab was about 31.25 bps/Hz, approximately 2.7 times higher than 2×2 MIMO operations with a 20 dB SNR reference level in a Rayleigh fading environment. Due to

better performances in bandwidth, isolation, total efficiency, channel capacity and radiation patterns, the proposed six-element MIMO array is a potential applicant for 5G smartphone systems.

Author Contributions: Conceptualization, M.A., S.H.K. and A.I.; methodology, M.A.; software, M.A, S.H.K. and A.I.; validation, M.A., L.F.A. and S.K. (Sunghwan Kim); formal analysis, A.I., M.A.B., S.K. (Shafiullah Khan) and S.K. (Sunghwan Kim); investigation, M.A., S.H.K., A.I. and L.F.A.; resources, L.F.A., A.I. and S.K. (Sunghwan Kim); data curation, A.I.; writing—original draft preparation, M.A. and S.H.K.; writing—review and editing, M.A., S.H.K., L.F.A., A.I., M.A.B., S.K. (Shafiullah Khan) and S.K. (Sunghwan Kim); visualization, A.I.; supervision, L.F.A. and S.K. (Sunghwan Kim); project administration, L.F.A., A.I. and S.K. (Sunghwan Kim); funding acquisition, S.K. (Sunghwan Kim).

Funding: This work (S2666095) was supported by project for Cooperative R&D between Industry, Academy, and Research Institute funded Korea Ministry of SMEs and Startups in 20.

Conflicts of Interest: The authors declare no conflict of interest.

References

- Iqbal, A.; Smida, A.; Mallat, N.K.; Ghayoula, R.; Elfergani, I.; Rodriguez, J.; Kim, S. Frequency and pattern reconfigurable antenna for emerging wireless communication systems. *Electronics* **2019**, *8*, 407. [[CrossRef](#)]
- Werner, K.; Furuskog, J.; Riback, M.; Hagerman, B. Antenna configurations for 4x4 MIMO in LTE-field measurements. In Proceedings of the 2010 IEEE 71st Vehicular Technology Conference, Taipei, Taiwan, 16–19 May 2010; pp. 1–5.
- Wang, Y.; Du, Z. A wideband printed dual-antenna system with a novel neutralization line for mobile terminals. *IEEE Antennas Wirel. Propag. Lett.* **2013**, *12*, 1428–1431. [[CrossRef](#)]
- Shoaib, S.; Shoaib, I.; Shoaib, N.; Chen, X.; Parini, C.G. MIMO antennas for mobile handsets. *IEEE Antennas Wirel. Propag. Lett.* **2014**, *14*, 799–802. [[CrossRef](#)]
- Guo, J.; Fan, J.; Sun, L.; Sun, B. A four-antenna system with high isolation for mobile phones. *IEEE Antennas Wirel. Propag. Lett.* **2013**, *12*, 979–982. [[CrossRef](#)]
- Ikram, M.; Hussain, R.; Sharawi, M.S. Low profile 6-element modified-monopole MIMO antenna system for mobile applications. In Proceedings of the 2016 IEEE International Symposium on Antennas and Propagation (APSURSI), Fajardo, Puerto Rico, 26 June–1 July 2016; pp. 73–74.
- Chen, Z.; Geyi, W.; Zhang, M.; Wang, J. A study of antenna system for high order MIMO device. *Int. J. Antennas Propag.* **2016**, *2016*. [[CrossRef](#)]
- Sharawi, M.; Jan, M.; Aloji, D. Four-shaped 2 × 2 multi-standard compact multiple-input–multiple-output antenna system for long-term evolution mobile handsets. *IET Microw. Antennas Propag.* **2012**, *6*, 685–696. [[CrossRef](#)]
- Anguera, J.; Andújar, A.; Mateos, R.M.; Kahng, S. A 4 × 4 MIMO multiband antenna system with non-resonant elements for smartphone platforms. In Proceedings of the 2017 11th European Conference on Antennas and Propagation (EUCAP), Paris, France, 19–24 March 2017; pp. 2705–2708.
- Moradikordalivand, A.; Leow, C.Y.; Rahman, T.A.; Ebrahimi, S.; Chua, T.H. Wideband MIMO antenna system with dual polarization for WiFi and LTE applications. *Int. J. Microw. Wirel. Technol.* **2016**, *8*, 643–650. [[CrossRef](#)]
- Malathi, C.; Thiripurasundari, D. CSRR Loaded 2x1 Triangular MIMO Antenna for LTE Band Operation. *Adv. Electromagn.* **2017**, *6*, 78–83. [[CrossRef](#)]
- Yang, B.; Chen, M.; Li, L. Design of a four-element WLAN/LTE/UWB MIMO antenna using half-slot structure. *AEU-Int. J. Electron. Commun.* **2018**, *93*, 354–359. [[CrossRef](#)]
- Wong, K.L.; Chen, Y.C.; Li, W.Y. Four LTE low-band smartphone antennas and their MIMO performance with user's hand presence. *Microw. Opt. Technol. Lett.* **2016**, *58*, 2046–2052. [[CrossRef](#)]
- Wong, K.L.; Kang, T.W.; Tu, M.F. Internal mobile phone antenna array for LTE/WWAN and LTE MIMO operations. *Microw. Opt. Technol. Lett.* **2011**, *53*, 1569–1573. [[CrossRef](#)]
- Wang, T.; Li, G.; Huang, B.; Miao, Q.; Fang, J.; Li, P.; Tan, H.; Li, W.; Ding, J.; Li, J.; et al. Spectrum analysis and regulations for 5G. In *5G Mobile Communications*; Springer: Berlin/Heidelberg, Germany, 2017; pp. 27–50.
- Anguera, J.; Sanz, I.; Mumbrú, J.; Puente, C. Multiband handset antenna with a parallel excitation of PIFA and slot radiators. *IEEE Trans. Antennas Propag.* **2009**, *58*, 348–356. [[CrossRef](#)]

17. Abedin, M.; Ali, M. Modifying the ground plane and its effect on planar inverted-F antennas (PIFAs) for mobile phone handsets. *IEEE Antennas Wirel. Propag. Lett.* **2003**, *2*, 226–229. [[CrossRef](#)]
18. Anguera, J.; Cabedo, A.; Picher, C.; Sanz, I.; Ribó, M.; Puente, C. Multiband handset antennas by means of groundplane modification. In Proceedings of the 2007 IEEE Antennas and Propagation Society International Symposium, Honolulu, HI, USA, 9–15 June 2007; pp. 1253–1256.
19. Hossa, R.; Byndas, A.; Bialkowski, M. Improvement of compact terminal antenna performance by incorporating open-end slots in ground plane. *IEEE Microw. Wirel. Components Lett.* **2004**, *14*, 283–285. [[CrossRef](#)]
20. Chang, T.H.; Kiang, J.F. Compact multi-band H-shaped slot antenna. *IEEE Trans. Antennas Propag.* **2013**, *61*, 4345–4349. [[CrossRef](#)]
21. Gabriel, C. Tissue equivalent material for hand phantoms. *Phys. Med. Biol.* **2007**, *52*, 4205. [[CrossRef](#)] [[PubMed](#)]
22. Certification, C. Test Plan for mobile station over the air performance. *Method Meas. Radiat. Power Receiv. Perform. Revis.* **2005**, *2*, 273–275.
23. Pelosi, M.; Franek, O.; Knudsen, M.; Pedersen, G. Influence of dielectric loading on PIFA antennas in close proximity to user's body. *Electron. Lett.* **2009**, *45*, 246–248. [[CrossRef](#)]
24. Plicanic, V.; Lau, B.K.; Ying, Z. Performance of a multiband diversity antenna with hand effects. In Proceedings of the 2008 International Workshop on Antenna Technology: Small Antennas and Novel Metamaterials, Chiba, Japan, 4–6 March 2008; pp. 534–537.
25. Bouazizi, A.; Zaibi, G.; Iqbal, A.; Basir, A.; Samet, M.; Kachouri, A. A dual-band case-printed planar inverted-F antenna design with independent resonance control for wearable short range telemetric systems. *Int. J. Microw. Comput. Eng.* **2019**, *29*, e21781. [[CrossRef](#)]
26. Ilvonen, J.; Valkonen, R.; Holopainen, J.; Kivekäs, O.; Vainikainen, P. Reducing the interaction between user and mobile terminal antenna based on antenna shielding. In Proceedings of the 2012 6th European Conference on Antennas and Propagation (EUCAP), Prague, Czech Republic, 26–30 March 2012; pp. 1889–1893.
27. Zhang, S.; Zhao, K.; Ying, Z.; He, S. Adaptive quad-element multi-wideband antenna array for user-effective LTE MIMO mobile terminals. *IEEE Trans. Antennas Propag.* **2013**, *61*, 4275–4283. [[CrossRef](#)]
28. Ding, Y.; Du, Z.; Gong, K.; Feng, Z. A novel dual-band printed diversity antenna for mobile terminals. *IEEE Trans. Antennas Propag.* **2007**, *55*, 2088–2096. [[CrossRef](#)]
29. Iqbal, A.; Saraereh, O.A.; Ahmad, A.W.; Bashir, S. Mutual coupling reduction using F-shaped stubs in UWB-MIMO antenna. *IEEE Access* **2017**, *6*, 2755–2759. [[CrossRef](#)]
30. Iqbal, A.; A Saraereh, O.; Bouazizi, A.; Basir, A. Metamaterial-based highly isolated MIMO antenna for portable wireless applications. *Electronics* **2018**, *7*, 267. [[CrossRef](#)]
31. Iqbal, A.; Basir, A.; Smida, A.; Mallat, N.K.; Elfergani, I.; Rodriguez, J.; Kim, S. Electromagnetic Bandgap Backed Millimeter-Wave MIMO Antenna for Wearable Applications. *IEEE Access* **2019**, *7*, 111135–111144. [[CrossRef](#)]
32. Ying, Z.; Bolin, T.; Plicanic, V.; Derneryd, A.; Kristensson, G. Diversity antenna terminal evaluation. In Proceedings of the 2005 IEEE Antennas and Propagation Society International Symposium, Washington, DC, USA, 3–8 July 2005; Volume 2, pp. 375–378.
33. Tian, R.; Lau, B.K.; Ying, Z. Multiplexing efficiency of MIMO antennas. *IEEE Antennas Wirel. Propag. Lett.* **2011**, *10*, 183–186. [[CrossRef](#)]
34. Kildal, P.S.; Rosengren, K. Correlation and capacity of MIMO systems and mutual coupling, radiation efficiency, and diversity gain of their antennas: simulations and measurements in a reverberation chamber. *IEEE Commun. Mag.* **2004**, *42*, 104–112. [[CrossRef](#)]

